Chinese Chemical Letters 33 (2022) 2687–2691

Contents lists available at ScienceDirect

Chinese Chemical Letters

journal homepage: www.elsevier.com/locate/cclet

Graphene aerogel supported Pt-Ni alloy as efficient electrocatalysts for alcohol fuel oxidation

Xiang Ding[a,b], Meng Li[b], Junling Jin[a], Xiaobing Huang[a], Xiang Wu[c], Ligang Feng[b,*]

[a] Hunan Provincial Key Laboratory of Water Treatment Functional Materials, College of Chemistry and Material Engineering, Hunan University of Arts and Science, Changde 415000, China
[b] School of Chemistry and Chemical Engineering, Yangzhou University, Yangzhou 225002, China
[c] School of Materials Science and Engineering, Shenyang University of Technology, Shenyang 110870, China

ARTICLE INFO

Article history:
Received 21 July 2021
Revised 20 September 2021
Accepted 23 September 2021
Available online 29 September 2021

Keywords:
PtNi
Fuel cells reaction
Graphene aerogel
Anti-poisoning effect
CO-stripping

ABSTRACT

Alcohol fuels oxidation plays a significant role in carbon sustainable cycling and high-performance catalyst with a strong anti-poisoning effect is desired. Herein, Pt-Ni alloy supported on the N-doped graphene aerogel synthesized by simple freeze-drying and annealing was demonstrated to have such catalytic ability for alcohol fuel oxidation. Pt-Ni alloy particles were found uniformly dispersed over the surface of 3D N-doped graphene aerogel. High anti-poisoning ability for CO-like intermediates oxidation was demonstrated by the CO-stripping experiment. The as-prepared catalyst was found to have outstanding catalytic performance for methanol and ethanol oxidation with high catalytic activity, stability and catalytic kinetics. Compared to the control samples, the improved catalytic ability could be due to the presence of oxophilic Ni species and the support effect of 3D N-doped graphene aerogel that combined multi-advantages of large surface area, facile mass transfer, and abundant defects.

© 2021 Published by Elsevier B.V. on behalf of Chinese Chemical Society and Institute of Materia Medica, Chinese Academy of Medical Sciences.

The carbon-neutral fuels have received increasing attention due to the environmental problems caused by fossil fuels consummation, and among the promising fuels, small molecular of C1 and C2 alcohol fuels are very promising liquid fuels used in the direct liquid fuel cells, that can be generated from the carbon dioxide reduction [1]. To realize the sustainable carbon cycle, liquid alcohol fuel oxidation is a significant section, and highly efficient catalysts are required to transfer the chemical energy to electricity *via* the electrochemical process [2]. Currently, the noble metal-based catalysts of Pt or Pd are still the most efficient electrocatalysts to catalyze the complicated oxidation process of methanol and ethanol fuels [3]. However, problems like the high cost, limited utilization and their poisoning issue caused by strongly adsorbed intermediates (carbon monoxide) are still faced in the current scientific research fields [4,5]. Therefore, much effort is required to increase the Pt utilization with high catalytic activity and the anti-poisoning ability for their application in the direct liquid fuel cells technique.

The current catalysts can be classified into the supported and non-supported catalysts, and the supported catalysts in the form of Pt-based active phase supported on the conductive carbon materials with a large surface area are commercially applied in the fuel cells technique [6,7]. This is because they have high active site exposure, dispersion and catalytic stability but low cost. The Pt-based active phase design should consider the bi-functional catalytic mechanism and the electronic effect, which explained the catalytic mechanism of alcohol fuel oxidation [8,9]. Alloying with cheap oxophilic metals is considered to be an effective way for the synthesis of high-performance electrocatalysts [10–12]. Based on the above-mentioned principles, the electron cloud density of Pt could be adjusted by adding other metals that can weaken the strength of the CO–Pt bond, and meanwhile, hydroxyl groups (OH_{ads}) groups offered by the adsorption sites of oxophilic metals can promote the CO species oxidation [13–15]. Among them, PtNi alloys exhibit enhanced electrocatalytic activity and high tolerance toward CO poisoning in an acidic environment for alcohol fuel oxidation [16]. To increase the catalytic efficiency, the active phase should be dispersed over the carbon support to enhance the interaction between the reactants, catalyst and the electrolyte in the three-phase interface [17].

The traditional conductive supports of Vulcan carbon, carbon nanotube have been largely employed for commercial application. Graphene that has excellent electrical and thermal conductivity, high mechanical strength is also employed for the catalysis reaction, while the thin two-dimensional sp^2-hybridized carbon network always results in the re-stacking and coalescing phenomenon, thereby leading to the less accessible surface area as support ma-

* Corresponding author.
E-mail address: ligang.feng@yzu.edu.cn (L. Feng).

https://doi.org/10.1016/j.cclet.2021.09.076
1001-8417/© 2021 Published by Elsevier B.V. on behalf of Chinese Chemical Society and Institute of Materia Medica, Chinese Academy of Medical Sciences.

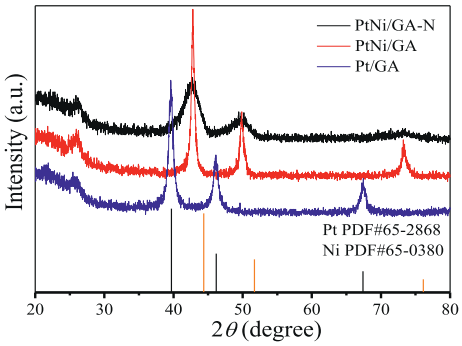

Fig. 1. XRD patterns of PtNi/GA-N, PtNi/GA and Pt/GA catalysts.

terials [18]. Graphene aerogels (GAs), assembled by the graphene nanosheets, have the favorable properties of graphene with high porosity and low density of aerogels. Therefore, they are suitable as support of 3D catalysts system construction [19]. Moreover, the catalytic property of graphene can be further increased by N doping due to the modified local electronic structure of the carbon polarization [20]. Compared to the pristine graphene, the N-doped graphene as noble catalyst support can offer more anchor sites for active phase formation and increase the synergistic effects of active phase and support for catalytic reactions [21,22]. For example, Pt nanoparticles supported on N-doped graphene obtained by different approaches were demonstrated to have improved catalytic activity in the electrochemical reactions for oxygen reduction and methanol oxidation [23,24]. Therefore, developing nitrogen-doped graphene aerogels as support is worth of try for catalytic performance improvement.

Considering the above-mentioned multi-functions, herein, we fabricated the 3-D N-doped graphene aerogel supported Pt-Ni alloy (PtNi/GA-N) for alcohols fuels oxidation. The as-prepared catalysts were characterized by a variety of physical characterization and measured by a series of electrochemical measurements. By comparing to some control samples, PtNi/GA-N was found to have the best catalytic performance for both methanol and ethanol oxidation. The high performance, based on the current research, was suggested to result from the multi-advantages integration of the large surface area, facile mass transfer, and abundant defects derived from N-doping and microporous structure.

To compare the catalytic performance and understand the synergism of multi-compositions in the system, the catalyst of Pt nanoparticles supported over the GA (Pt/GA), PtNi nanoalloys supported over the GA (PtNi/GA), and PtNi nanoalloys supported over the N doped graphene (PtNi/GA-N) were fabricated and evaluated for the catalytic reactions. The crystal structure of the as-obtained catalysts was probed by powder X-Ray diffraction (XRD). The peak at 26° is observed for all the samples that could be assigned to (002) facet of the graphene support (Fig. 1). The characteristic peaks of fcc structured Pt are observed on the Pt/GA samples, where 2θ values of 39.66°, 46.16°, 67.37° are attributed to the (111), (200) and (220) crystal planes (PDF#65-2868). While no prominent peaks can be assignable to monometallic Pt or Ni in the XRD patterns for PtNi/GA-N and PtNi/GA catalysts due to the formation of PtNi alloy. Specifically, the 2θ values of the diffraction peaks for PtNi/GA-N and PtNi/GA catalysts are around 42.6°, 49.8° and 73.3°, corresponding to the (111), (200) and (220) facets of a face-centered cubic (fcc) lattice [25,26]. The 2θ values of these peaks sit between those of pure Pt and Ni, indicating the formation of the Pt-Ni alloy resulting from the shortened Pt-Pt bond by incorporating the smaller Ni atoms into the Pt crystal lattice. Moreover, the crystal size calculated by the Scheer equation based on the peak of 42.6° (111) is 3.9 nm for PtNi/GA-N catalyst, smaller

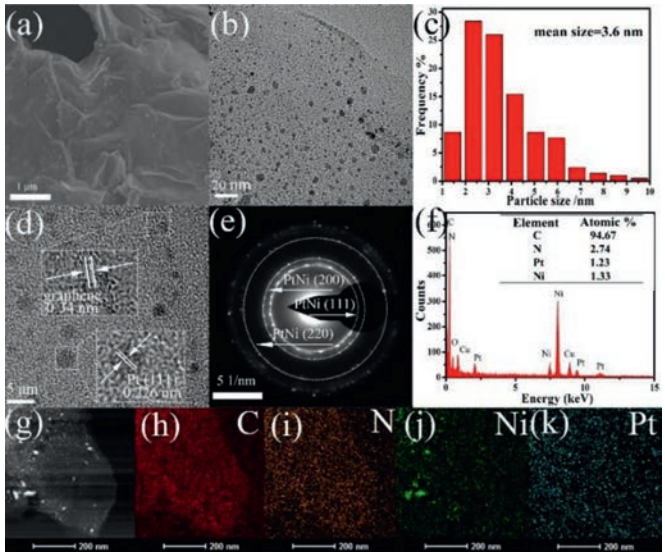

Fig. 2. (a) SEM images of PtNi/GA-N catalyst. (b) TEM image of PtNi/GA-N catalyst. (c) Particle size distribution histogram of PtNi/GA-N catalyst. High-resolution TEM (d), SAED (e) and EDS (f) of PtNi/GA-N catalyst. (g) STEM and elemental mapping images of the PtNi/GA-N catalyst, (h) C, (i) N, (j) Ni, (k) Pt.

than that of PtNi/GA and Pt/GA. The N-doped graphene aerogel can offer more defects and anchoring sites for the PtNi alloy formation compared to graphene aerogel alone, therefore, small particle size was found due to the good dispersion and efficient anchoring sites induced by N-doping. The small particle size could expose more electrochemically active surface area and active sites, which is beneficial to the following catalytic reactions.

The morphology of the PtNi/GA-N catalyst was further characterized by scanning electron microscope (SEM) and transmission electron microscope (TEM). The 3D graphene network is observed in the SEM image for all the catalysts (Fig. 2a and Fig. S1 in Supporting information for other samples). The Pt-Ni alloy particles dispersed over the surface of the graphene aerogel can be seen in the TEM image (Fig. 2b). The average particle size of 3.6 nm is indicated in the particle size distribution histogram (Fig. 2c). In the high-resolution TEM (HRTEM) image (Fig. 2d), a lattice spacing of 0.226 nm can be ascribed to the (111) facet of Pt-Ni alloy and the lattice spacing of 0.34 nm is from the graphene layer. The selected area electron diffraction (SAED) pattern shows a polycrystalline character with some evident spots and rings (Fig. 2e), which can be indexed to the (111), (200) and (220) planes of PtNi alloy. The energy-dispersive X-ray detector spectrum (EDS) shows the presence of Pt, Ni, C, N and O elements (Fig. 2f), and the ratio of Pt/Ni in the catalyst was measured to be 1. The elemental distribution of Pt, Ni, C and N is shown in the element mapping images (Figs. 2g–k). Specifically, nitrogen is found uniformly doped into the graphene nanosheet, and several particles of Pt–Ni alloy are found on the graphene surface.

The surface chemical state of PtNi/GA-N catalyst was probed by X-ray photoelectron spectroscopy (XPS). The whole binding energy was calibrated by the main peak of C 1s at 284.6 eV (Fig. S2 in Supporting information) [27]. The structure of N-doped graphene can be supported by the C–N bond in the C 1s and N 1s spectra (Figs. S2 and S3 in Supporting information). Specifically, the N 1s spectrum could be ascribed to the pyridinic N, pyrrolic N and graphitic N [28]. The high-resolution spectrum of Pt 4f has two peaks of $4f_{7/2}$ and Pt $4f_{5/2}$, and they can be deconvoluted into metallic Pt and oxidized Pt (Pt^{2+}) based on the chemical valence [5,29,30]. The peaks at 71.3 eV and 74.6 eV are attributed to metallic Pt, and those peaks at 72.3 eV and 75.6 eV can be assigned to

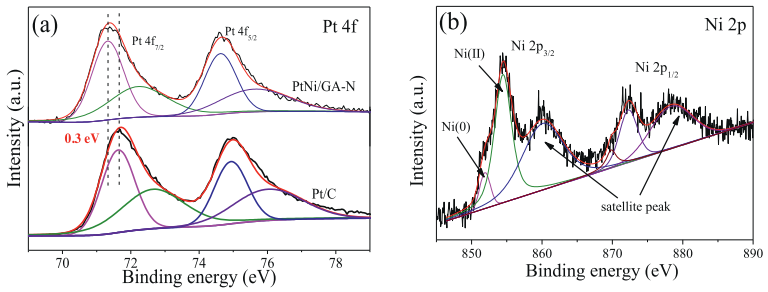

Fig. 3. XPS spectra of (a) Pt 4f for PtNi/GA-N and a commercial Pt/C catalyst and (b) Ni 2p for PtNi/GA-N catalyst.

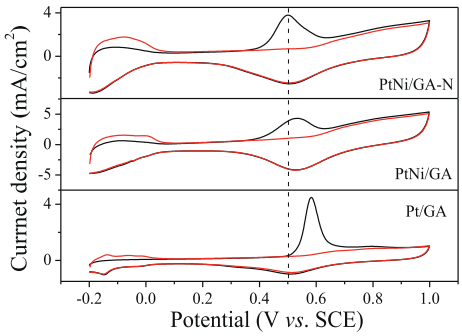

Fig. 4. CO stripping voltammograms of PtNi/GA-N, PtNi/GA and Pt/GA catalysts in 0.5 mol/L H_2SO_4 solutions at a scan rate of 20 mV/s.

Pt^{2+} species in PtO and $Pt(OH)_2$ (Table S1 in Supporting information). Compared to the commercial Pt-C catalyst, those peaks shift to the low binding energy direction by about 0.3 eV (Fig. 3a), indicating an electron-enrich surface state of Pt. The strong adsorption of CO on Pt as CO-Pt will occupy the Pt active sites causing the reduced catalytic performance due to active site poisoning. The electrons enriched surface of Pt would induce the downshift of d-band center, which would consequently weaken the adsorption of CO and promote CO oxidation and desorption [31,32]. Thus, the increased anti-CO poisoning was obtained. The high-resolution spectrum of Ni 2p has two components of $2p_{3/2}$ and $2p_{1/2}$, and each component can be deconvoluted into the metallic Ni, surface oxidized Ni^{2+} and the accompanied satellite peak (Fig. 3b). Specifically, the peaks of 851.9 eV and 869.8 eV are for the metallic Ni from the PtNi alloy; the peaks at 854.4 eV and 872.3 eV are attributed to Ni^{2+} resulted from the surface oxidation, that concurred well with the reports elsewhere for the PtNi alloy [33].

As know that the adsorption of poisoning intermediates will reduce the catalytic performance, and the anti-poisoning ability is very significant to the high-performance catalyst [34,35]. Here, the anti-poisoning ability can be probed *via* the CO-stripping technique by evaluating the onset and peak oxidation potential of adsorbed CO (CO_{ads}). The lower the potentials for CO_{ads} oxidation, the higher the anti-poisoning ability. The PtNi/GA-N catalyst was found to have the best performance compared to PtNi/GA and Pt/GA catalysts (Fig. 4). To be specific, the peak potential for CO_{ads} oxidation is 0.50 V, 0.53 V and 0.58 V for PtNi/GA-N, PtNi/GA and Pt/GA catalyst, respectively. The potential was 30 mV and 80 mV lower than that of PtNi/GA and Pt/GA catalysts, respectively. Similar cases were observed for the onset potentials (Table S2 in Supporting information). It can be seen that Pt/GA has the lowest CO-tolerance ability, and the performance can be largely improved by forming PtNi alloy due to the oxophilic character of Ni; the N-doped GA support could further increase the anti-poisoning ability as indicated by 30 mV potentials less due to the electronic structure modification of carbon. The composite results thus make PtNi/GA-N have the best performance. Beside, the ECSA was calculated to be 83 m^2/g for PtNi/GA-N catalyst, which was the largest ECSA compared with the PtNi/GA (71 m^2/g) and Pt/GA (55 m^2/g) catalysts. The higher the ECSA, the more reactive sites available, and the higher the catalytic activity. The improved poisoning-tolerance ability could be due to the synergistic effect between the Pt-Ni alloy and the N-doped graphene aerogel.

Following that, we evaluated the catalytic performance of these catalysts for alcohol fuel oxidation. The electrochemical behavior of PtNi/GA-N, PtNi/GA and Pt/GA catalysts was compared in the background electrolyte of 0.5 mol/L H_2SO_4, and polycrystalline Pt behaviors were observed for all the electrodes (Fig. S4 in Supporting information). When evaluated for methanol oxidation, the best performance is found in the PtNi/GA-N catalyst judged by the peak current density (Fig. 5a). Specifically, the peak current density is measured to be 91.2 mA/cm^2, about 2.1 times of PtNi/GA catalyst (43.5 mA/cm^2), 2.8 times of Pt/GA catalyst (32.8 mA/cm^2) and 3.3 times of a commercial 20% Pt/C catalyst (27.3 mA/cm^2). Moreover, the smallest onset potential for methanol oxidation is also observed on PtNi/GA-N catalyst, which is consistent with the trend found for the ability of CO_{ads} oxidation. Mass activity and specific activity were also calculated for the catalytic performance evaluation (Fig. S5 in Supporting information). PtNi/GA-N catalyst still shows the highest catalytic activity, and the maximum mass activity was calculated to be 1132.4 mA/mg_{Pt}, much higher than that of PtNi/GA (543.82 mA/mg_{Pt}) and Pt/GA (406.19 mA/mg_{Pt}) catalysts. The maximum specific activity is 1.36 mA/cm^2, about 1.77 times of the PtNi/GA catalyst and 1.84 times of the Pt/GA catalyst. The catalyst performance is also much higher than some graphene-supported Pt-based catalysts like Pt-graphene [36], 3D Pt/RuO_2/graphene [37] and graphene-based nitrogen-doped porous carbon-PtZn [38]. The influence of the scan rate on the catalytic performance of methanol oxidation was investigated (Fig. S6 in Supporting information), and the peak current density is gradually increased accompanying the positive shift of the peak potential with the increase of the scan rates. A diffusion process-controlled reaction is indicated by the linear relationship of the peak current vs. the square root of scan rate (Fig. 5b). The large slope value indicates a faster electron transfer rate in the rate-determining step [39], and correspondingly, PtNi/GA-N catalyst possesses the faster catalytic kinetics. This result is also further supported by the kinetics analysis obtained from the Tafel slope (Fig. S7 in Supporting information). The Tafel slope of PtNi/GA-N is 86 mV/dec, smaller than that of PtNi/GA and Pt/GA catalyst, indicating a much faster catalytic kinetics. Electrochemical impedance spectroscopy (EIS) was probed to evaluate the charge transfer ability for methanol oxidation at 0.4 V (Fig. 5c), and the diameter of the arc reflects the charge transfer ability. The smallest diameter of arc is observed on PtNi/GA-N catalyst indicating the lowest charge transfer resistance (R_{ct}). The specific value of R_{ct} can be obtained by fitting the Nyquist plot using a typical equivalent circuit (inset of Fig. 5c). The uncompensated solution resistance for all the electrodes is *ca.*

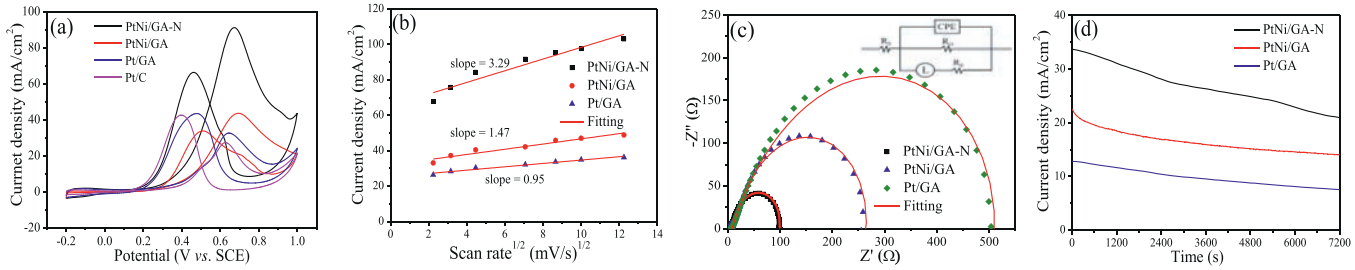

Fig. 5. (a) Cyclic voltammetry curves of PtNi/GA-N, PtNi/GA Pt/GA and commercial Pt/C (20 wt%) catalysts in 0.5 mol/L H_2SO_4/1 mol/L CH_3OH solution at a scan rate of 50 mV/s. (b) The plot of anodic peak current density *vs.* the square root of scan rate. (c) Nyquist plots of PtNi/GA-N, PtNi/GA and Pt/GA catalysts (inset for equivalent circuit). (d) Chronoamperometry curves of PtNi/GA-N, PtNi/GA and Pt/GA catalysts in 0.5 mol/L H_2SO_4/1 mol/L CH_3OH solution.

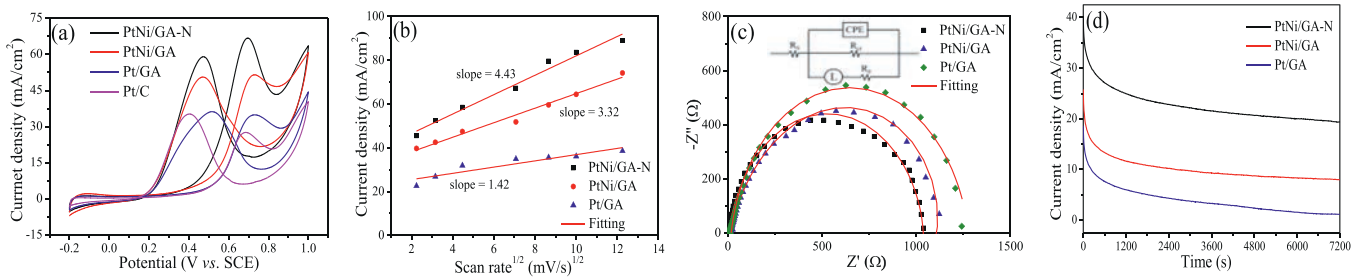

Fig. 6. (a) Cyclic voltammetry curves of PtNi/GA-N, PtNi/GA Pt/GA and commercial Pt/C (20 wt%) catalysts in 0.5 mol/L H_2SO_4/1 mol/L CH_3CH_2OH solution at a scan rate of 50 mV/s. (b) The plot of anodic peak current density *vs.* the square root of scan rate. (c) Nyquist plots of PtNi/GA-N, PtNi/GA and Pt/GA catalysts (inset for equivalent circuit). (d) Chronoamperometry curves of PtNi/GA-N, PtNi/GA and Pt/GA catalysts in 0.5 mol/L H_2SO_4/1 mol/L CH_3CH_2OH solution.

6.8 Ω, and the smallest R_{ct} of 109 Ω is found on the PtNi/GA-N catalyst, indicating its largely improved catalytic kinetics (Table S4 in Supporting information). The stability of the catalyst for methanol oxidation was probed by a chronoamperometry (CA) test for two hours at 0.5 V (Fig. 5d). The current density for all the catalysts is reduced slowly with time. The final current density is 21.1 mA/cm^2 for PtNi/GA-N catalyst, which is 1.5 and 2.8 times of PtNi/GA and Pt/GA catalysts, respectively. The current retention rate after 2 h for PtNi/GA-N catalyst is 64%, higher than that of PtNi/GA (61%) and Pt/GA (58%). The high catalytic stability consistently supported the high anti-CO poisoning ability. Thus, PtNi/GA-N catalysts have high catalytic activity and stability for methanol oxidation.

The ethanol oxidation, an attractive fuel for proton exchange membrane fuel cells, was also investigated and a similar trend for the catalytic performance was obtained. As shown in the CV measurements (Fig. 6a), the highest forward peak current density of about 66.8 mA/cm^2 is observed for PtNi/GA-N catalyst, which is about 1.3, 1.9 and 2.4 times higher than that of PtNi/GA (51.3 mA/cm^2), Pt/GA (35 mA/cm^2) and Pt/C (27.6 mA/cm^2), respectively. Moreover, PtNi/GA-N has a much lower onset potential than that of PtNi/GA and Pt/GA catalyst, indicating the improved kinetics for the electro-oxidation of ethanol. The highest catalytic efficiency expressed by the mass activity and the specific activity is still found on the PtNi/GA-N catalyst (Fig. S8 in Supporting information). Specifically, the mass activity and specific activity of PtNi/GA-N catalyst are 832.7 mA/mg$_{Pt}$ and 1 mA/cm^2, respectively, higher than that of PtNi/GA and Pt/GA catalysts.

The improved catalytic activity was also well supported by the catalytic kinetics analysis. By analyzing the peak current density *versus* the square root of scan rate, the linear relationship was also obtained for this catalyst (Fig. 6b and Figs. S9a-c in Supporting information), and the largest slope value was obtained on the PtNi/GA-N catalyst indicating its fastest catalytic kinetics. Meanwhile, Tafel slope and impedance analysis consistently supported the improved catalytic kinetics. To be specific, the Tafel slope of PtNi/GA-N is 81 (Fig. S10 in Supporting information), lower than the reference samples, indicating the water dissociation as the rate-determining step [40]; The R_{ct} is 1046 Ω for the PtNi/GA-N catalyst, that is the smallest value among the concerned catalysts (Fig. 6c and Table S6 in Supporting information). The catalytic stability for ethanol oxidation was also evaluated, and the final current density of PtNi/GA-N catalyst is 19.6 mA/cm^2 after 2 h, about 2.4 and 17.8 times of PtNi/GA and Pt/GA catalysts, respectively (Fig. 6d). In other words, about 52% of the current is kept for PtNi/GA-N catalyst, much higher than that of PtNi/GA (31%) and Pt/GA (7%) catalysts. Thus, PtNi/GA-N catalyst possessed high anti-CO poisoning ability during the catalytic process.

In summary, a three-dimensional N-doped graphene aerogel supported Pt-Ni alloy was reported active for alcohol fuel of methanol and ethanol oxidation resulting from multi-components synergism. PtNi alloy nanoparticles with a small average particle size of 3.6 nm were found uniformly distributed over the 3D N-doped graphene aerogel. The obtained catalysts showed much higher anti-CO poisoning ability and catalytic performance for alcohol fuel oxidation compared to the control samples. Much higher catalytic abilities in terms of catalytic stability, kinetic and charge transfer capability were also observed for the PtNi/GA-N catalyst. The high catalytic performance was attributed to the large accessible surface area and favorable mass transfer channel from GA support and the ultrafine PtNi alloy nanoparticles supported over their surface. The combined advantages from the oxophilic Ni species and the support effect of 3D N-doped graphene aerogel are thus instructive for highly efficient catalyst design and fabrication.

Declaration of competing interest

The authors declare that they have no known competing financial interests or personal relationships that could have appeared to influence the work reported in this paper.

Acknowledgments

This work was supported by the Hunan Provincial Natural Science Foundation of China (No. 2019JJ50411) and the Scientific Re-

search Fund of Hunan University of Arts and Science (No. 20ZD02). The work was also supported by the National Natural Science Foundation of China (Nos. 21972124, 21603041). We thank Yufei Bao for the experimental assistance and discussion.

Supplementary materials

Supplementary material associated with this article can be found, in the online version, at doi:10.1016/j.cclet.2021.09.076.

References

[1] X. Zhao, H. Zhao, J. Sun, G. Li, R. Liu, Chin. Chem. Lett. 31 (2020) 1782–1786.
[2] B. Fang, Z. Liu, Y. Bao, L. Feng, Chin. Chem. Lett. 31 (2020) 2259–2262.
[3] W. Guo, X. Yao, L. Peng, et al., Chin. Chem. Lett. 31 (2020) 836–840.
[4] T. Radhakrishnan, N. Sandhyarani, Electrochim. Acta 298 (2019) 835–843.
[5] Y. Zhou, D. Liu, W. Qiao, et al., Mater. Today Phys. 17 (2021) 100357.
[6] L. Tao, S. Dou, Z. Ma, S. Wang, Electrochim. Acta 157 (2015) 46–53.
[7] X. Yang, J. Xue, L. Feng, Chem. Commun. 55 (2019) 11247–11250.
[8] J. Zhang, S. Lu, Y. Xiang, S.P. Jiang, ChemSusChem 13 (2020) 2484–2502.
[9] N. Bhuvanendran, S. Ravichandran, W. Zhang, et al., Int. J. Hydrog. Energy 45 (2020) 6447–6460.
[10] W. Gong, Z. Jiang, R. Wu, et al., Appl. Catal. B: Environ. 246 (2019) 277–283.
[11] Q. Wang, S. Chen, H. Lan, et al., J. Mater. Chem. A 7 (2019) 18143–18149.
[12] Y. Zhou, D. Liu, Z. Liu, L. Feng, J. Yang, ACS Appl. Mater. Interfaces 12 (2020) 47065–47075.
[13] J. Li, S. You, M. Liu, et al., Appl. Catal. B: Environ. 265 (2020) 118574.
[14] Y. Bao, M. Zha, P. Sun, G. Hu, L. Feng, J. Energy Chem. 59 (2021) 748–754.
[15] H. Liu, D. Yang, Y. Bao, X. Yu, L. Feng, J. Power Sources 434 (2019) 226754.
[16] N. Cheng, L. Zhang, H. Jiang, et al., Nanoscale 11 (2019) 16945–16953.
[17] W.S. Jung, J. Energy Chem. 27 (2018) 326–334.
[18] X.L. Sui, L.M. Zhang, L. Zhao, et al., Int. J. Hydrog. Energy 43 (2018) 21899–21907.
[19] Y. Bao, L. Feng, Acta Phys. Chim. Sin. 37 (2021) 2008031.
[20] T. Schiros, D. Nordlund, L. Pálová, et al., Nano Lett. 12 (2012) 4025–4031.
[21] Y. Zhang, F. Gao, P. Song, et al., ACS Sustain. Chem. Eng. 7 (2019) 3176–3184.
[22] X. Zhu, Z. Hu, M. Huang, et al., Chin. Chem. Lett. 32 (2021) 2033–2037.
[23] Y. Xin, J.G. Liu, X. Jie, et al., Electrochim. Acta 60 (2012) 354–358.
[24] B. Xiong, Y. Zhou, R. O'Hayre, Z. Shao, Appl. Surf. Sci. 266 (2013) 433–439.
[25] N.N. Kariuki, W.J. Khudhayer, T. Karabacak, D.J. Myers, ACS Catal. 3 (2013) 3123–3132.
[26] R. Lin, X. Cai, Z. Hao, H. Pu, H. Yan, Electrochim. Acta 283 (2018) 764–771.
[27] M. Li, Y. Gu, Y. Chang, et al., Chem. Eng. J. 425 (2021) 130686.
[28] C. Pei, R. Ding, X. Yu, L. Feng, ChemCatChem 11 (2019) 4617–4623.
[29] H. Liu, D.W. Yang, Y.F. Bao, X. Yu, L.G. Feng, J. Power Sources 434 (2019) 226754.
[30] X. Teng, A. Shan, Y. Zhu, R. Wang, W.M. Lau, Electrochim. Acta 353 (2020) 136542.
[31] Q. Lv, X. Ren, L. Liu, W. Guan, A. Liu, Ionics 26 (2020) 1325–1336.
[32] K. Jiang, H.X. Zhang, S.Z. Zou, W.B. Cai, Phys. Chem. Chem. Phys. 16 (2014) 20360–20376.
[33] T.C. Deivaraj, W. Chen, J.Y. Lee, J. Mater. Chem. 13 (2003) 2555–2560.
[34] W. Chen, J. Xue, Y. Bao, L. Feng, Chem. Eng. J. 381 (2020) 122752.
[35] Y. Bao, H. Liu, Z. Liu, F. Wang, L. Feng, Appl. Catal. B: Environ. 274 (2020) 119106.
[36] L. Dong, R.R.S. Gari, Z. Li, M.M. Craig, S. Hou, Carbon 48 (2010) 781–787.
[37] H. Huang, J. Zhu, D. Li, et al., J. Mater. Chem. A 5 (2017) 4560–4567.
[38] X. Yuan, Y. Min, J. Wu, L. Xu, W. Yue, Electrochim. Acta (2021) 139106.
[39] G. Li, L. Feng, J. Chang, et al., ChemSusChem 7 (2014) 3374–3381.
[40] J. Flórez-Montaño, G. García, O. Guillén-Villafuerte, et al., Electrochim. Acta 209 (2016) 121–131.